

Band alignment of p-type oxide/ε-Ga_2O_3 heterojunctions investigated by x-ray photoelectron spectroscopy

Chang Rao(饶畅), Zeyuan Fei(费泽元), Weiqu Chen(陈伟驱), Zimin Chen(陈梓敏), Xing Lu(卢星), Gang Wang(王钢), Xinzhong Wang(王新中), Jun Liang(梁军), Yanli Pei(裴艳丽)

Citation: Chin. Phys. B . 2020, 29(9): 097303 . **doi:** 10.1088/1674-1056/ab9c0d
Journal homepage: http://cpb.iphy.ac.cn; http://iopscience.iop.org/cpb

What follows is a list of articles you may be interested in

Emerging properties of two-dimensional twisted bilayer materials

Yang Cheng(程阳), Chen Huang(黄琛), Hao Hong(洪浩), Zixun Zhao(赵子荀), Kaihui Liu(刘开辉)

Chin. Phys. B . 2019, 28(10): 107304 . **doi:** 10.1088/1674-1056/ab3e46

Energy band alignment at Cu_2O/ZnO heterojunctions characterized by *in situ* x-ray photoelectron spectroscopy

Yan Zhao(赵妍), Hong-Bu Yin(尹泓卜), Ya-Jun Fu(符亚军), Xue-Min Wang(王雪敏), Wei-Dong Wu(吴卫东)

Chin. Phys. B . 2019, 28(8): 087301 . **doi:** 10.1088/1674-1056/28/8/087301

Analysis of displacement damage effects on bipolar transistors irradiated by spallation neutrons

Yan Liu(刘岩), Wei Chen(陈伟), Chaohui He(贺朝会), Chunlei Su(苏春垒), Chenhui Wang(王晨辉), Xiaoming Jin(金晓明), Junlin Li(李俊霖), Yuanyuan Xue(薛院院)

Chin. Phys. B . 2019, 28(6): 067302 . **doi:** 10.1088/1674-1056/28/6/067302

Optoelectronic properties of bottom gate-defined in-plane monolayer WSe_2 p-n junction

Di Liu(刘頓), Xiao-Zhuo Qi(祁晓卓), Kuei-Lin Chiu(邱奎霖), Takashi Taniguchi, Xi-Feng Ren(任希锋), Guo-Ping Guo(郭国平)

Chin. Phys. B . 2018, 27(8): 087303 . **doi:** 10.1088/1674-1056/27/8/087303

Abundant photoelectronic behaviors of $La_{0.67}Sr_{0.33}MnO_3$/Nb: $SrTiO_3$ junctions

Hai-Lin Huang(黄海林), Deng-Jing Wang(王登京), Hong-Rui Zhang(张洪瑞), Hui Zhang(张慧), Chang-Min Xiong(熊昌民), Ji-Rong Sun(孙继荣), Bao-Gen Shen(沈保根)

Chin. Phys. B . 2017, 26(7): 077302 . **doi:** 10.1088/1674-1056/26/7/077302

Band alignment of p-type oxide/ε-Ga_2O_3 heterojunctions investigated by x-ray photoelectron spectroscopy*

Chang Rao(饶畅)[1], Zeyuan Fei(费泽元)[1], Weiqu Chen(陈伟驱)[1], Zimin Chen(陈梓敏)[1], Xing Lu(卢星)[1], Gang Wang(王钢)[1], Xinzhong Wang(王新中)[2], Jun Liang(梁军)[3], and Yanli Pei(裴艳丽)[1,2,†]

[1] *School of Electronics and Information Technology, State Key Laboratory of Optoelectronics Materials & Technologies, Sun Yat-Sen University, Guangzhou* 510006, *China*

[2] *Department of Electronic Communication and Technology, Shenzhen Institute of Information Technology, Shenzhen* 518172, *China*

[3] *School of Advance Materials, Peking University Shenzhen Graduated School, Shenzhen* 518055, *China*

(Received 25 March 2020; revised manuscript received 27 May 2020; accepted manuscript online 12 June 2020)

The ε-Ga_2O_3 p–n heterojunctions (HJ) have been demonstrated using typical p-type oxide semiconductors (NiO or SnO). The ε-Ga_2O_3 thin film was heteroepitaxial grown by metal organic chemical vapor deposition (MOCVD) with three-step growth method. The polycrystalline SnO and NiO thin films were deposited on the ε-Ga_2O_3 thin film by electron-beam evaporation and thermal oxidation, respectively. The valence band offsets (VBO) were determined by x-ray photoelectron spectroscopy (XPS) to be 2.17 eV at SnO/ε-Ga_2O_3 and 1.7 eV at NiO/ε-Ga_2O_3. Considering the bandgaps determined by ultraviolet-visible spectroscopy, the conduction band offsets (CBO) of 0.11 eV at SnO/ε-Ga_2O_3 and 0.44 eV at NiO/ε-Ga_2O_3 were obtained. The type-II band diagrams have been drawn for both p–n HJs. The results are useful to understand the electronic structures at the ε-Ga_2O_3 p–n HJ interface, and design optoelectronic devices based on ε-Ga_2O_3 with novel functionality and improved performance.

Keywords: ε-Ga_2O_3, x-ray photoelectron spectroscopy (XPS), valence band offset, band alignment

PACS: 73.40.Lq, 82.80.Pv, 73.20.At, 73.61.Le **DOI:** 10.1088/1674-1056/ab9c0d

1. Introduction

Recently, Ga_2O_3 as a wide bandgap semiconductor has drawn intense attention. It has an extremely wide bandgap (4.6–4.9 eV), and a theoretical breakdown electric field as high as 8 MV/cm.[1–3] Thus, it has the potential in deep-ultraviolet optical devices and power devices.[4–8] There are five different polymorphic structures of Ga_2O_3, including α-, β-, γ-, δ-, and ε-phases. Among them, ε-Ga_2O_3 has drawn lots of attention. Compared with β-Ga_2O_3 often reported, hexagonal ε-Ga_2O_3 is compatible with other hexagonal semiconductors such as GaN and SiC.[9] Furthermore, it has been theoretically predicted that there is a strong spontaneous polarization effect, which could form a high-mobility two-dimensional electron gas (2DEG) in ε-Ga_2O_3-based heterostructures.[10] Therefore, high-breakdown-voltage, high-mobility, and low-cost optoelectronics could be realized using ε-Ga_2O_3.[7,11]

In our previous work, high-quality ε-Ga_2O_3 film with a layer-by-layer morphology was grown on *c*-plane sapphire by metal-organic chemical vapor deposition (MOCVD).[12] However, Ga_2O_3 is an intrinsically doped n-type semiconductor with lower formation energy of donors related to the oxygen vacancies compared to that of acceptor ions.[1] Although, some literature studies exist on the experimental work to realize p-type conductivity Ga_2O_3 by doping with Mg, Zn, and Mg–Zn, it is very difficult to achieve.[13–15] As a result, Ga_2O_3 based p–n homojunction has not been realized. It will prevent the optoelectronic devices design. Fortunately, some oxides are intrinsically p-type semiconductors with intrinsic accepted defects, the ε-Ga_2O_3 based p–n heterojunction (HJ) can be proposed with these typical p-type oxide semiconductors.

The p–n HJ band alignment is an important part of device design and applications. It can be divided into 3 types: type I also called straddling type, type-II the staggered type, and type-III the broken type.[16–18] At present, there are many studies on the band alignment of β-Ga_2O_3 p–n HJs. The results are dependent on the HJ fabrication process and the materials. Li *et al.* have reported a type-I band alignment of Li-doped NiO and Si-doped β-Ga_2O_3.[19] Ghosh *et al.* have reported that sol-gel fabricated NiO on single crystal β-Ga_2O_3 had type-II band alignment, α-Cr_2O_3 on single crystal β-Ga_2O_3 was the same.[20,21] However, the band alignment of the ε-Ga_2O_3 p–n HJ is not clear, which is crucial to design ε-Ga_2O_3 optoelectronic devices with novel function and improved performance.

In this work, ε-Ga_2O_3 was heteroepitaxial grown on *c*-axis sapphire substrate by MOCVD with three-step growth method. The ε-Ga_2O_3 p–n HJs were demonstrated using NiO and SnO, which are the most representative p-type ox-

*Project supported by the National Natural Science Foundation of China (Grant No. 61774172), the Guangdong Provincial Department of Science and Technology, China (Grant Nos. 2019B010132002 and 2016B090918106), the Pengcheng Scholar Funding (2018), and Shenzhen Science and Technology Innovation Committee, China (Grant No. KQJSCX20180323174713505).

†Corresponding author. E-mail: peiyanli@mail.sysu.edu.cn

© 2020 Chinese Physical Society and IOP Publishing Ltd

ide semiconductors.[22–25] The energy band alignment of these HJs was investigated by x-ray photoelectron spectroscopy (XPS).

2. Experiment

The ε-Ga_2O_3 thin films were grown on *c*-axis sapphire substrates by MOCVD using a three-step growth method. Triethylgallium (TEGa) was used as the precursor of Ga, and the deionized water (H_2O) and nitrous oxide (N_2O) were used as the precursors of O in different steps, while argon was the carrier gas. First, the buffer layer was grown at 550 ℃ with TEGa flow rate of 90 sccm and H_2O flow rate of 2000 sccm for 30 min under processing pressure of 100 torr. The second epitaxy layer was grown at 600 ℃ for 60 min under chamber pressure of 20 torr, where N_2O was used as the precursor of O with flow rate of 500 sccm. After that, the third epitaxy layer was grown at temperature of 640 ℃ for 60 min, while all precursors flow rates remained the same.

SnO films were deposited by electron-beam evaporation with substrate temperature of 280 ℃ using SnO_2 as the target under a high vacuum of 4.5×10^{-6} torr. This method has been described in literature in detail.[26] NiO thin film was prepared by thermal oxidation. At first, a Ni thin film was deposited by electron beam evaporation under room temperature. Then, the thermal oxidation of the Ni layer was performed by rapid thermal annealing (RTA) for 10 min in O_2 ambient with flow rate of 0.3 slpm. According to the deposition rate and time, we precisely controlled the thickness of the SnO and NiO thin films.

Table 1. The samples.

Sample	Structure
1	100 nm ε-Ga_2O_3 on sapphire
2	75 nm SnO on glass
3	3 nm SnO on ε-Ga_2O_3
4	40 nm NiO on sapphire
5	3 nm NiO on ε-Ga_2O_3

In this study, five samples were prepared in order to investigate the valence band offsets (ΔE_v) of the SnO/ε-Ga_2O_3 and NiO/ε-Ga_2O_3 HJs using XPS, respectively. They are sample 1: ε-Ga_2O_3 thin film on the *c*-axis sapphire substrate with thickness of 100 nm, which represents the properties corresponding to the bulk ε-Ga_2O_3, sample 2: SnO film on glass with thickness of 75 nm, sample 3: SnO on bulk ε-Ga_2O_3 with thickness of 3 nm, sample 4: NiO film on sapphire wafer with thickness of 40 nm, and sample 5: NiO thin film on bulk ε-Ga_2O_3 with thickness of 3 nm. Samples 1, 2, and 4 were used to obtain the valence band maximum (VBM) and core level (CL) positions, while samples 3 and 5 were used to obtain the CL offset between the p-type oxides and ε-Ga_2O_3. The sample information is summarized in Table 1. The XPS instrument is ESCALAB 250 of thermos-VG Scientific with monochromat Al *K* x-radiation at source excitation energy of 15 keV.

3. Results and discussion

Figure 1(a) shows the x-ray diffraction (XRD) pattern of sample 1. Expect for the sapphire (0006) peak, the other three peaks are all attributed to ε-Ga_2O_3.[12] Figure 1(b) shows the high-resolution XRD rocking curve for the (004) plane. A full width at half maximum (FWHM) of 648 arcsec is observed. Based on the rocking curve of ε-Ga_2O_3 (004), the calculated density of screw dislocations is 2.55×10^8 cm^{-2}. The results indicate that the pure ε-Ga_2O_3 with high crystal quality is fabricated by MOCVD with the three-step growth method.

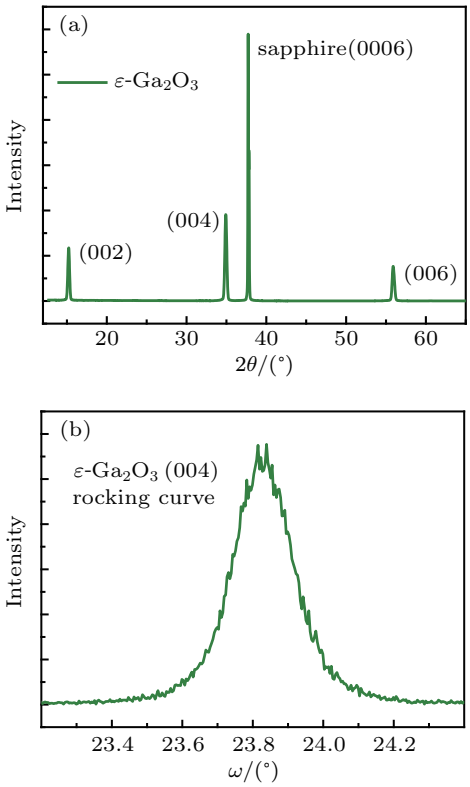


Fig. 1. (a) The XRD pattern of the Ga_2O_3 thin film on *c*-axis sapphire substrate and (b) the rocking curve for the (004) plane.

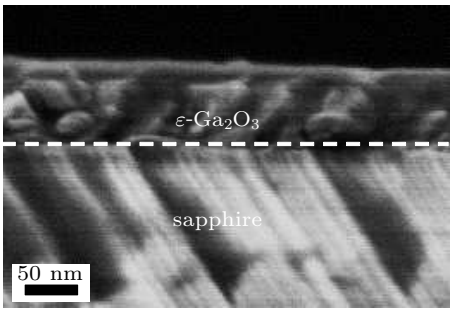


Fig. 2. Cross-sectional SEM image of the ε-Ga_2O_3 thin film on sapphire.

In this work, the NiO and SnO thin films were fabricated by electron-beam evaporation with excellent coverage. There-

fore, the roughness of the interface between ε-Ga_2O_3 and p-type oxides is mainly determined by the ε-Ga_2O_3 thin film surface roughness. Figure 2 is the cross-sectional SEM image of the ε-Ga_2O_3 thin film on sapphire. It is observed that the surface is smooth. It is consistent with our previous results. In our previous work, we have reported that the ε-Ga_2O_3 thin film grown by layer-by-layer mode has an atomic flat surface.[12]

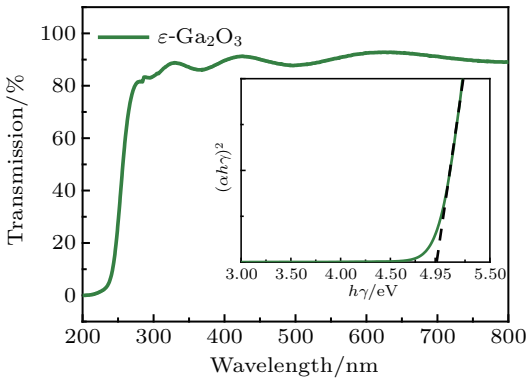


Fig. 3. The transmission spectrum of the Ga_2O_3 thin film on c-axis sapphire substrate. The inset shows the optical bandgap calculation procedure.

Figure 3 shows the transmission spectrum of the ε-Ga_2O_3 thin film in the wavelength range from 200 nm to 800 nm. The optical bandgap can be extrapolated according to the formula

$$\alpha h\gamma = A(h\gamma - E_g)^n,$$

where α stands for the absorption coefficient, $h\gamma$ stands for the photon energy, A is a constant, and E_g is the optical bandgap. As the ε-Ga_2O_3 thin film has a direct bandgap structure, the n value of 0.5 is used. The fitting result shows that the optical bandgap of the ε-Ga_2O_3 is $\sim$ 4.95 eV. The value is basically consistent with our previous results.

Figure 4(a) shows the XRD pattern of sample 2 (SnO). The c-axis preferred orientation α-SnO thin film is confirmed.[27] Figure 4(b) is the transmission spectrum of the SnO thin film. The direct optical bandgap is evaluated as 2.89 eV using the $(\alpha h\gamma)^2$ versus $h\gamma$ plot, as shown in Fig. 4(b). The result is consistent with our previous work.[26]

The XRD pattern and transmission spectra of the NiO thin film, which was grown on glass, are shown in Figs. 4(c) and 4(d), respectively. It suggests a polycrystalline NiO film (JCPDS card No. 47-1049) with a direct bandgap of $\sim$ 3.69 eV consistent with the literature. The bandgap of NiO has been reported at the range of 3.6–4.0 eV.[25]

Hall effect measurements have been employed to confirm the conductive mode of the SnO and NiO thin films. The results indicate that both NiO and SnO films are p-type semiconductors with hole concentration of $\sim 10^{17}$ cm^{-3}.

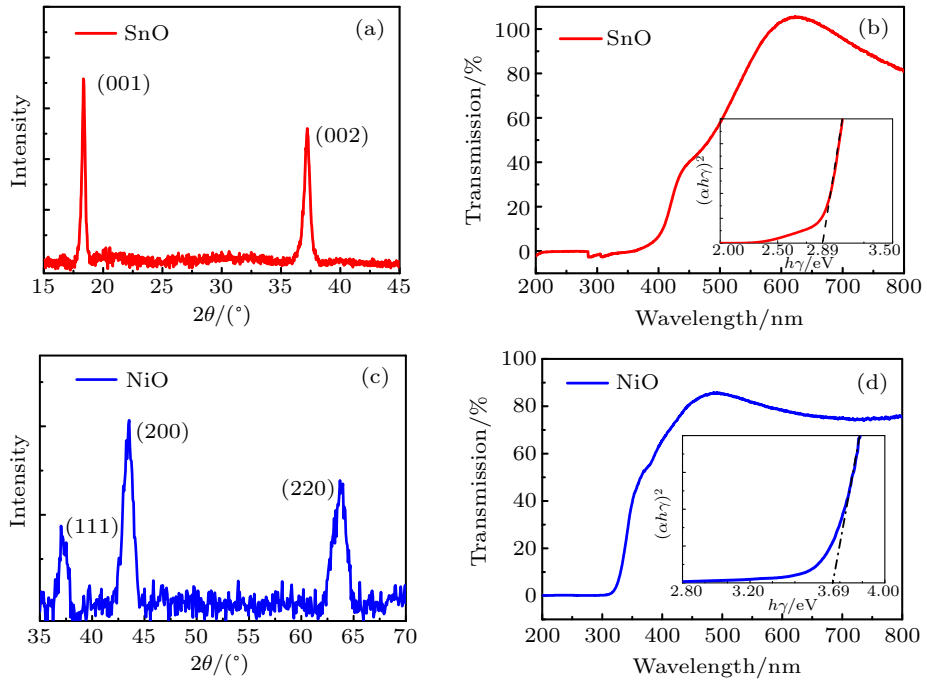


Fig. 4. (a) The XRD pattern and (b) transmittance spectra of the SnO thin film on glass. (c) The XRD pattern of the NiO thin film on glass, (d) the transmittance spectra of the NiO thin film on sapphire. The insets of (c) and (d) show their optical bandgaps.

Figure 5 shows the XPS data of sample 1 (ε-Ga_2O_3), indicating the VBM and Ga 2p core level (CL). Note that all XPS results have been calibrated by taking the C 1s peak at 284.8 eV. The value of the VBM has been determined to be 2.94 ± 0.02 eV by linear extrapolation of the leading VBM edge to the base line of the VB spectra. The obtained VBM value is far away from the Fermi level, indicating the n-type nature of the ε-Ga_2O_3. The binding energy (BE) of Ga 2p is found to be 1117.61 ± 0.01 eV, and $(E_{Ga2p} - E_{VBM})_{Ga2O3}$ is 1114.67 ± 0.03 eV. In contrast, as shown in Fig. 6(a), the

VBM of the SnO thin film (sample 2) has been determined to be 0.77 ± 0.02 eV, which is close to the Fermi level, indicating the p-type nature of the SnO layer. The BE of Sn 3d and $(E_{\mathrm{Sn3d}} - E_{\mathrm{VBM}})_{\mathrm{SnO}}$ have been found to be 486.52 ± 0.01 eV and 485.75 ± 0.03 eV, respectively. The BE difference between the CLs of Sn 3d and Ga 2p has been calculated to be 631.09 ± 0.02 eV by measurement of sample 3 which has an ultra-thin SnO layer on top. It allows us to collect photoelectrons from both top and bottom layers. The measurement data is summarized in Table 2.

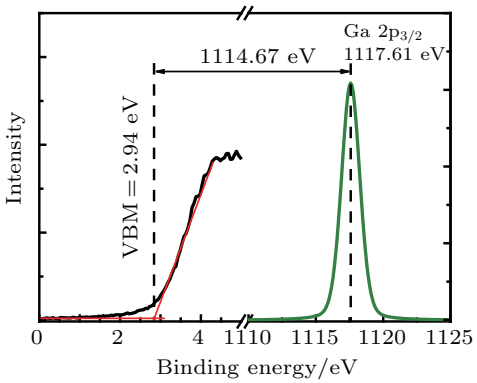


Fig. 5. High resolution XPS spectra of sample 1, it shows the Ga 2p CL and VBM.

The valence band offsets (ΔE_{v}) of the SnO /ε-Ga_2O_3 HJ is calculated based on Kraut's method by following formula:[28]

$$\Delta E_{\mathrm{v}}(\mathrm{SnO}/\mathrm{Ga_2O_3}) = \left(E_{\mathrm{Ga2p}} - E_{\mathrm{v}}\right)_{\mathrm{Ga_2O_3}} - \left(E_{\mathrm{Sn3d}} - E_{\mathrm{v}}\right)_{\mathrm{SnO}} - \left(E_{\mathrm{Ga2p}} - E_{\mathrm{Sn3d}}\right)_{\mathrm{SnO/Ga_2O_3}}.$$

The $\Delta E_{\mathrm{v}}(\mathrm{SnO}/\mathrm{Ga_2O_3})$ is extracted to be 2.17 ± 0.08 eV. Combining with the optical band gap, we draw the energy band diagram of SnO/ε-Ga_2O_3 HJ in Fig. 5(c). It shows a type-II band alignment with a large VBO (2.17 ± 0.08 eV) and a small CBO (0.11 ± 0.08 eV).

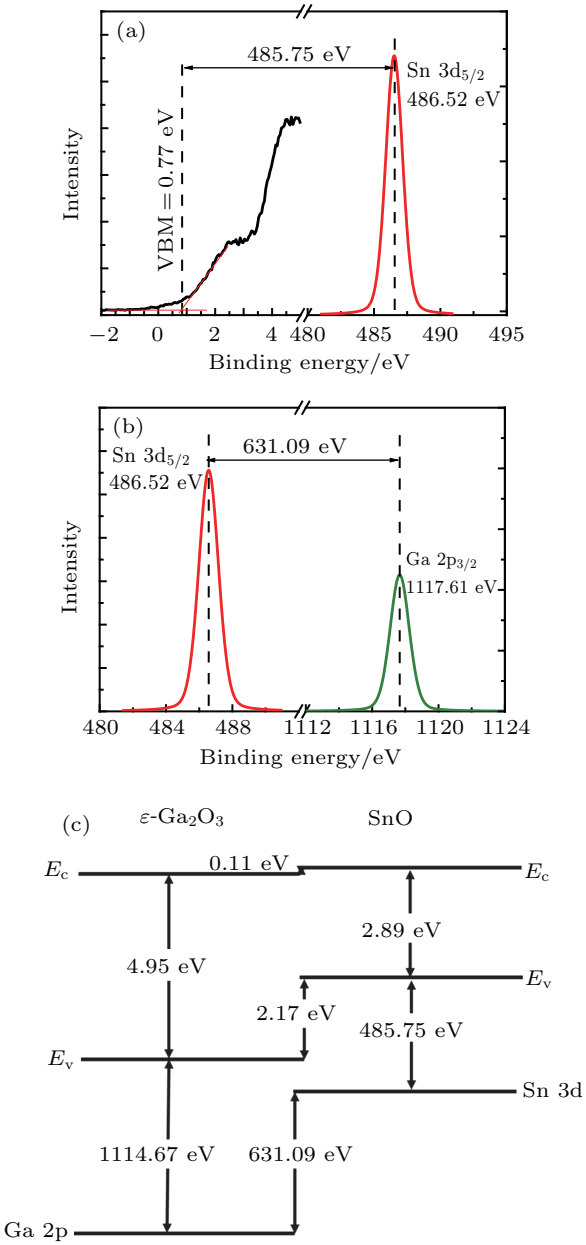


Fig. 6. High resolution XPS spectra for (a) sample 2 and (b) sample 3. (c) Schematic diagram for band alignment of the SnO/ε-Ga_2O_3 interface.

Table 2. Summarize of calculation results.

	Sample	Optical band gap/eV		CL/eV	VBM/eV	Valence band offset/eV
SnO/ε-Ga_2O_3	1	4.95	Ga 2p	1117.61 ± 0.01	2.94 ± 0.02	2.17 ± 0.08
	2	2.89	Sn 3d	486.52 ± 0.01	0.77 ± 0.02	
	3		Ga 2p	1117.61 ± 0.01		
			Sn 3d	486.52 ± 0.01		
NiO/ε-Ga_2O_3	1	4.95	Ga 2p	1117.61 ± 0.01	2.94 ± 0.02	1.7 ± 0.08
	4	3.69	Ni 2p	854.07 ± 0.01	0.63 ± 0.02	
	5		Ga 2p	1117.39 ± 0.01		
			Ni 2p	854.46 ± 0.01		

Figure 7(a) shows the XPS data of sample 4 (NiO) including the VBM and Ni 2p CL.[29] The obtained VBM of the NiO thin film is 0.63 ± 0.02 eV, which is close to the Fermi level, indicating the p-type nature of the NiO layer. The BE of Ni 2p is found to be 854.07 ± 0.01 eV, and $(E_{\mathrm{Ni2p}} - E_{\mathrm{VBM}})_{\mathrm{NiO}}$ is 853.44 ± 0.03 eV. The BE difference between the CLs of Ni 2p and Ga 2p has been measured to be 262.93 ± 0.02 eV with sample 5. The measurement data is shown in Table 2.

The ΔE_v of NiO/ε-Ga_2O_3 HJ is extracted to be 1.7 ± 0.08 eV according to Kraut's formula

$$\Delta E_v(\mathrm{NiO}/\mathrm{Ga_2O_3}) = \left(E_{\mathrm{Ga2p}} - E_v\right)_{\mathrm{Ga_2O_3}} - \left(E_{\mathrm{Ni2p}} - E_v\right)_{\mathrm{NiO}} - \left(E_{\mathrm{Ga2p}} - E_{\mathrm{Ni2p}}\right)_{\mathrm{NiO/Ga_2O_3}}.$$

The energy band alignment of NiO/ε-Ga_2O_3 HJ is drawn in Fig. 7(c) using the optical band gap value in Table 2. Like SnO/ε-Ga_2O_3 HJ, the NiO/ε-Ga_2O_3 HJ also has a type-II band alignment with 1.7 ± 0.08 eV VBO and 0.44 ± 0.08 eV CBO. The result is close to the report by Ghosh *et al.* that NiO/β-Ga_2O_3 has type-II band alignment with VBO of 1.6 eV, and CBO of 0.3 eV.[21]

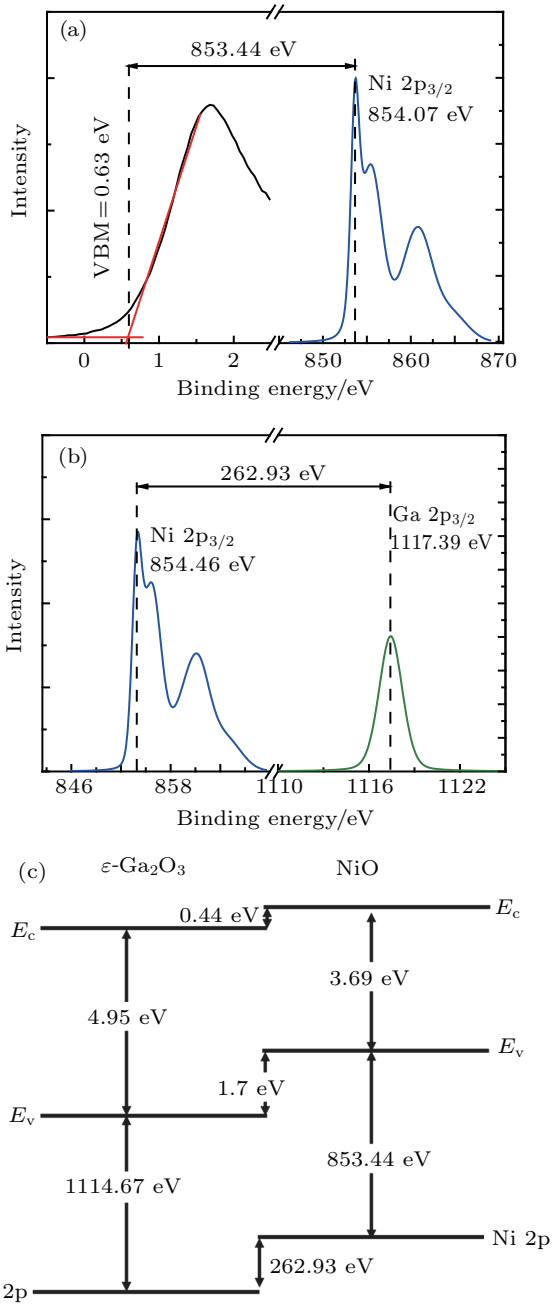


Fig. 7. High resolution XPS spectra for (a) sample 4 and (b) sample 5. (c) Schematic diagram for band alignment of the NiO/ε-Ga_2O_3 interface.

The type-II band alignment makes HJs suitable for device applications based on the separation of charge carriers. We can choose appropriate HJ structures according to specific applications. The turn-on voltage is mainly dominated by the value of ΔE_c. A small ΔE_c will provide a low turn-on voltage, which leads to higher forward current, but also a higher leakage current at ambient temperature. An appropriate value of ΔE_c is desirable for the optimum performance of a p–n HJ diode. Compared with SnO/ε-Ga_2O_3 with smaller ΔE_c of 0.11 eV, the NiO/ε-Ga_2O_3 with ΔE_c of 0.44 eV is suitable for p–n diode application with lower leakage current. On the other hand, the larger ΔE_v in SnO/ε-Ga_2O_3 (2.17 eV) makes it suitable as a hole blocking layer in p–n HJ based UV LEDs.[30,31] In addition, when the junction is in a positive bias, compared with the NiO/ε-Ga_2O_3 HJ, the SnO/ε-Ga_2O_3 HJ with smaller ΔE_c and larger ΔE_v will provide high electron injection efficiency to improve the performance of bipolar transistors.

4. Conclusions

In this work, p-type semiconductor thin films of NiO and SnO were fabricated on MOCVD growing ε-Ga_2O_3, respectively. The valence band offsets of NiO/ε-Ga_2O_3 and SnO/ε-Ga_2O_3 HJs were investigated by XPS measurement. Combined with the measurements of the optical bandgaps, the band alignment diagrams were drawn. Both SnO/ε-Ga_2O_3 and NiO/ε-Ga_2O_3 HJs have type-II band alignment. The HJs are suitable for device applications due to the advantage for the separation of charge carriers.

References

[1] Pearton S J, Yang J, Cary P H, Ren F, Kim J, Tadjer M J and Mastro M A 2018 *Appl. Phys. Rev.* **5** 011301
[2] Kuramata A, Koshi K, Watanabe S, Yamaoka Y, Masui T and Yamakoshi S 2016 *Jpn. J. Appl. Phys.* **55** 1202A2
[3] Baldini M, Albrecht M, Fiedler A, Irmscher K, Schewski R and Wagner G 2017 *ECS J. Solid State Sci. Technol.* **6** Q3040
[4] Watahiki T, Yuda Y, Furukawa A, Yamamuka M, Takiguchi Y and Miyajima S 2017 *Appl. Phys. Lett.* **111** 222104
[5] Nakagomi S, Hiratsuka K, Kakuda Y and Yoshihiro K 2017 *ECS J. Solid State Sci. Technol.* **6** Q3030
[6] Guo D, Wu Z, Li P, An Y, Liu H, Guo X, Yan H, Wang G, Sun C, Li L and Tang W 2014 *Opt. Mater. Express* **4** 1067
[7] Pavesi M, Fabbri F, Boschi F, Piacentini G, Baraldi A, Bosi M, Gombia E, Parisini A and Fornari R 2018 *Mater. Chem. Phys.* **205** 502
[8] Qin Y, Long S, Dong H, He Q, Jian G, Zhang Y, Hou X, Tan P, Zhang Z, Lv H, Liu Q and Liu M 2019 *Chin. Phys. B* **28** 18501
[9] Xia X, Chen Y, Feng Q, Liang H, Tao P, Xu M and Du G 2016 *Appl. Phys. Lett.* **108** 202103
[10] Cho S B and Mishra R 2018 *Appl. Phys. Lett.* **112** 162101
[11] Zhuo Y, Chen Z, Tu W, Ma X, Pei Y and Wang G 2017 *Appl. Surf. Sci.* **420** 802
[12] Chen Z, Li Z, Zhuo Y, Chen W, Ma X, Pei Y and Wang G 2018 *Appl. Phys. Express* **11** 101101
[13] Ho Q D, Frauenheim T and Deák P 2018 *J. Appl. Phys.* **124** 145702
[14] Kyrtsos A, Matsubara M and Bellotti E 2018 *Appl. Phys. Lett.* **112** 032108

[15] Neal A T, Mou S, Rafique S, Zhao H, Ahmadi E, Speck J S, Stevens K T, Blevins J D, Thomson D B, Moser N, Chabak K D and Jessen G H 2018 *Appl. Phys. Lett.* **113** 062101
[16] Cai C F, Wu H Z, Si J X, Jin S Q, Zhang W H, Xu Y and Zhu J F 2010 *Chin. Phys. B* **19** 77301
[17] Chang S H, Chen Z Z, Huang W, Liu X C, Chen B Y, Li Z Z and Shi E W 2011 *Chin. Phys. B* **20** 116101
[18] Zeng Y, Kuo C I, Hsu C, Najmzadeh M, Sachid A, Kapadia R, Yeung C, Chang E, Hu C and Javey A 2015 *IEEE Trans. Nanotechnol.* **14** 580
[19] Li K H, Alfaraj N, Kang C H, Braic L, Hedhili M N, Guo Z, Ng T K and Ooi B S 2019 *ACS Appl. Mater. Interfaces* **11** 35095
[20] Ghosh S, Baral M, Kamparath R, Choudhary R J, Phase D M, Singh S D and Ganguli T 2019 *Appl. Phys. Lett.* **115** 061602
[21] Ghosh S, Baral M, Kamparath R, Singh S D and Ganguli T 2019 *Appl. Phys. Lett.* **115** 251603
[22] Ogo Y, Hiramatsu H, Nomura K, Yanagi H, Kamiya T, Hirano M and Hosono H 2008 *Appl. Phys. Lett.* **93** 032113
[23] Nomura K, Kamiya T and Hosono H 2011 *Adv. Mater.* **23** 3431
[24] Liu A, Liu G, Zhu H, Shin B, Fortunato E, Martins R and Shan F 2016 *Appl. Phys. Lett.* **108** 233506
[25] Reddy A M, Reddy A S, Lee K S and Reddy P S 2011 *Solid State Sci.* **13** 314
[26] Pei Y, Liu W, Shi J, Chen Z and Wang G 2016 *J. Electron. Mater.* **45** 5967
[27] Liang L Y, Liu Z M, Cao H T and Pan X Q 2010 *ACS Appl. Mater. Interfaces* **2** 1060
[28] Kraut E A, grant R W, Waldrop J R and Kowalczyk S P 1980 *Phys. Rev. Lett.* **44** 1620
[29] Biesinger M C, Payne B P, Lau L W M, Gerson A and Smart R S C 2009 *Surf. Interface Anal.* **41** 324
[30] Varghese A, Thakar D, Jindal K, Ghosh V, Medhekar S and Saurabh 2020 *Nano Lett.* **20** 1707
[31] Marschall R 2014 *Adv. Funct. Mater.* **24** 2421